

Research Paper

## Mechanical Alloying and Spark Plasma Sintering of Equiatomic AlCoCrFeMnNi High Entropy Alloy

Farhad Abdi<sup>1</sup>, Hossein Aghajani<sup>1,2\*</sup>, Shahin Khameneh Asl<sup>1</sup>

1. Department of Materials Engineering, University of Tabriz, Tabriz, Iran.

2- School of Metallurgy and Materials Engineering, Iran University of Science and Technology, Tehran, Iran.

---

### ARTICLE INFO

---

#### Article history:

Received 11 September 2021  
Accepted 22 December 2021  
Available online 1 January 2022

#### Keywords:

*AlCoCrFeNiMn high entropy alloy*  
*Mechanical alloying*  
*Spark plasma sintering*

---

### ABSTRACT

---

In this research, a high entropy alloy of AlCoCrFeNiMn is made through mechanical alloying and the spark plasma sintering processes. Ball milling was done at different times of 12 h, 36 h, and 48 h in a cup with a diameter of 20 cm. Ball to powder percent weight of 10:1 was selected. X-ray diffraction patterns indicate the formation of solid solution microstructure after 48 h. The crystal size decreases from 23 to 16 nm with increasing milling time. The lattice strain of the structure increments from 0.3 to 0.68% with increasing time up to 48 h. SEM images clearly show the phenomenon of powder agglomeration and the absence of intermetallic compounds or brittle, complex structures. It is observed that with increasing ball-milling time, homogenization of powders increases, and the body-centered cubic phase is formed in the structure. The mechanically alloyed powders were consolidated spark plasma sintered at 700, 900, and 1000 °C. 50 MPa pressure, argon gas as atmosphere, and ten minutes as sintering time were selected as the sintering process parameters. The X-ray diffraction pattern shows that the structure of consolidated high entropy alloy has face-centered cubic and body-centered cubic phases. After sintering by the spark plasma method, the density of powders was measured by Archimedes' rules, and the value was determined as 99% of theoretical density. The structure was without porosity. The hardness was measured using the microhardness Vickers test. Loading force was 50 g and loading time was seven seconds. The highest hardness was about 649 HV<sub>0.05</sub>.

---

**Citation:** Abdi, F.; Aghajani, H; Khameneh Asl, Sh. (2022) Mechanical Alloying and Spark Plasma Sintering of Equiatomic AlCoCrFeMnNi High Entropy Alloy, Journal of Advanced Materials and Processing, 10 (1), 27-38. Dor: 20.1001.1.2322388.2022.10.1.3.6

#### Copyrights:

Copyright for this article is retained by the author (s), with publication rights granted to Journal of Advanced Materials and Processing. This is an open – access article distributed under the terms of the Creative Commons Attribution License (<http://creativecommons.org/licenses/by/4.0>), which permits unrestricted use, distribution and reproduction in any medium, provided the original work is properly cited.



---

\* **Corresponding Author**

E-mail Address: haghajani@iust.ac.ir

## 1. Introduction

To develop new materials for the aerospace, automotive, and rail industries, scientists are trying to find materials and alloys that have improved and desired properties. High Entropy Alloys (HEA) were first introduced as a new concept in the design and production of alloys [1-3]. High entropy alloys are a new level of metal alloys. Unlike conventional alloys that are consisted of one or two main metal elements, these alloys contain at least five or more metal elements in the range of 5-35 atomic percentages.

High entropy alloys are widely used in the transportation and energy industries due to their low density and high strength. High entropy alloys are an excellent alternative to titanium and steel alloys [4]. Among the remarkable properties of HEAs, low diffusion and strength stability have received much attention at high temperatures. In the form of a rod or powder, HEAs can be coated on the surfaces of tools and other components as surface hardening materials. The thermal spray or plasma arc process is used for surface hardening [4].

High entropy alloy possesses several properties, including high strength, thermal stability, wear resistance, and corrosion resistance. These alloys have the highest configurational entropy. This parameter plays a significant role in the organization of solid solutions. The formation of a solid solution depends on some parameters, such as the melting point, the synthesis temperature, and the interaction between the atoms. They are known as multipurpose element alloys (MPEAS), concentrated solid alloys (CSAs), and complex composite alloys (CCAs) [5, 6]. High entropy alloys (HEAs) are based on four inherent properties: First, the entropy effect, which reinstates the solid solution formation. Second is the effect of lattice distortion, which mainly affects the properties. Third, the impact of slow diffusion reduces the diffusion kinetics, and fourth, the effect of alloying elements, which have a combined impact on the final properties. The CoCrFeNiMn alloy is one of the first HEAs alloys extensively investigated because of its excellent physical properties, among cryogenic properties [7], thermodynamic stability [8], and other properties.

It has been reported that the CoCrFeNiMn alloy microstructure includes only BCC solid solution. Although CoCrFeNiMn alloy has excellent properties, it does not have high mechanical properties [9]. Aluminum may improve mechanical properties and result in a higher lattice distortion. He et al. [10] confirmed that increasing the amount of Al increases the yield strength and reduces the density. The strengthening mechanism is via establishing a BCC solid solution phase [11, 12]. Also, Hall-Petch

effects and refined grains play an essential role in this mechanism [13].

The HEAs have excellent corrosion resistance. By controlling the synthesis process, FCC, BCC, or an amorphous phase can be achieved, which leads to excellent corrosion resistance. In particular, combining some elements, including Cr, Ni, Co, and Cu, can increase the corrosion resistance of these alloys [14]. HEAs are made by melt casting [14-19, 21], mechanical alloying, high-energy ball milling [20, 22], and sputtering or molecular beam epitaxy (MBE) [23].

Many studies have been conducted on these alloys' synthesis and composition after normal melting and solidification. These benefits include good density in the specimens, no gas vacancies, and the removal of harmful contaminants from other elements. However, melting creates coarse grains ( $\geq 4\mu\text{m}$ ) with a heterogeneous structure during solidification [24]. The other method is powder metallurgy. A combination of mechanical alloying (MA) and sintering processes is prevalent in producing high entropy alloys. This method has a wide range of applications. In mechanical alloys (MA), solid solutions are formed at room temperature, and a homogeneous alloy is formed.

The mechanical alloying (MA) process presents many challenges in preparing HEA powders, including contamination during milling, oxidation, and a limited ability to shape [25]. The phase is observed to change with increasing rotation speed and the use of balls of different diameters. Phase transformation occurs when energy is transferred to the powders. High energy is very effective in achieving a Nano-crystalline structure in the powders [26]. The material of the milling cup also affects the type of phases. As an example, the CoCrFeNiMn alloy exhibits a single-phase FCC structure when synthesized using a WC cup and ball [27], while the BCC phase appears in the structure when synthesized using a stainless-steel cup and balls [28]. This may be due to the presence of chromium in the stainless steel. The FCC or BCC phase formation is related to reactive powders' processing condition and composition. He et al. [29] examined the impacts of Al addition on the microstructure and tensile strength of FeCoCrNiMn HEA. He et al. [29] reported that regarding the Al-containing HEA alloy, when the Al amount exceeded to 16%, the microstructure changed from the initial FCC to a single BCC structure. CoCrFeNiMnAl alloy made by mechanical alloying demonstrates FCC phase upon annealing at 500 °C. The FCC and BCC phases are created after Spark Plasma Sintering (SPS) process [30]. The powder metallurgy process makes it possible to achieve Nano-sized particles, which

improves the mechanical properties. A comparison of induction melting and powder metallurgy shows that powder metallurgy is an excellent and preferred process in producing HEAs. In powder metallurgy, grain refining occurs during mechanical alloying so that these particles are kept together during sintering. While in the melting and induction method, the grains are coarse and non-uniform. The milled alloys must be compacted to become a high-density structure with acceptable operational properties. Sintering is selected mainly to achieve a combination of density and crystalline structure. SPS is one of the most widely used techniques for sintering powders, despite some limitations such as C contamination and small sample sizes with most SPS units. Alloy powders are first pressurized and then heated to be condensed. Other methods such as hot vacuum pressing (HVPS) [31-35], Beam microwave sintering (BMS) [36], and hot isostatic pressing (HIP) [37] are also used for sintering [38, 39]. Some parameters, such as short process times, make the SPS method superior to the other methods mentioned. As a result, there is less time for grain growth, and the grains can be easily compacted to nano-crystalline size [40]. Studies have demonstrated that applying the maximum pressure at higher temperatures results in better adhesion and bonding of powder particles. This leads to achieving greater flexibility [40]. Comparing microwave sintering and SPS methods shows that the first method creates a large amount of porosity in

AlCoCrFeNi high entropy alloy, which affects the mechanical properties [41]. So, it can be concluded that SPS is the preferred method for sintering HEA powder.

In this research, the mechanical alloying (MA) method was used to make an AlCoCrFeNiMn alloy powder. After that, spark plasma sintering (SPS) was applied to powders, and the structure and phases formed at different sintering temperatures were characterized.

## 2. Experimental procedure

The production of AlCoCrFeNiMn alloy involves a few steps. In the first step, 99% pure powders of Al, Co, Mn, Ni, and Fe were prepared (Table 1). After determining the ratios required to achieve an equiatomic ratio, the required values were weighed on a high precision scale (0.0001g). Powders were then fed into a ball milling chamber and milled at different speeds. A stainless-steel chamber with a diameter of 10 cm was used in the mill process. And the balls were made of stainless steel. The ball to the powder weight percent (BPR) was selected as 10: 1. The mill was set at a rotational speed of 120 rpm. In this process, ethanol and alcohol were used as a process control agent (PCA). The powder mixture was milled at different times of 12 h, 36 h, and 48 h for mechanical alloying.

**Table 1.** Amounts and specifications of powder elements used to make AlCoCrFeNiMn alloy.

No	Element	Purity (%)	Size ( $\mu\text{m}$ )	Wt. %	Made by
1	Al	$\geq 99$	20 $\geq$	8.77	Germany
2	Co	$\geq 99$	10 $\geq$	19.17	Germany
3	Cr	$\geq 99$	63 $\geq$	16.89	South Korea
4	Fe	$\geq 99$	45	18.19	Germany
5	Mn	$\geq 99$	63 $\geq$	18.19	South Korea
6	Ni	$\geq 99$	75	17.87	Russia

The plasma spark sintering process was used to consolidate powders which were prepared after 48 h of ball milling. The sintering temperatures were selected 700, 900, and 1000 ° C. Sintering was performed in a vacuum atmosphere with average pressure 1.5 Pa. The axial pressure was 50 MPa, and the temperature rate was 50 °C / minute. The sample was maintained for ten minutes and then cooled in an argon atmosphere to ambient temperature.

The crystal structure of milled powders and sintered alloys was investigated by Bruker AXS, Advance D8, and Cu K $\alpha$  X-ray devices. The scanning 2 $\theta$  range

was from 20 to 100 degrees. The scanning speed was 0.1 degrees per second. After SPS, the resulting alloys were studied again by X-Ray diffraction. The microstructure of the sintered samples was studied with an optical microscope CARL-ZEISS-4996387, and images with a magnification of 100 $\times$  were prepared.

The mechanically alloyed powders and SPS synthesized alloys were investigated by ROVENTEC Vega TESCAN MIRA3 scanning electron microscope. The density of sintered alloys at different temperatures was determined using

Archimedes' principles. The hardness of the sintered alloy specimens was measured by the hardness Vickers MX-96604-BUEHLER micro-hardness tester. Vickers micro-hardness tester (MHVN) was used with a force of 50 g and a loading time of 15 seconds.

### 3. Results and discussion

#### 3.1. Mechanically alloyed powder

Figure 1 illustrates the XRD patterns of as-milled AlCoCrFeMnNi powders combined at different milling times. At the angles of  $2\theta=38^\circ$  peak of Al,  $2\theta=43^\circ$  peak of Mn,  $2\theta=45^\circ$  peak of Co, Cr, Ni, Fe, and Al,  $2\theta=49^\circ$  peak of Co and Mn,  $2\theta=53^\circ$  peak of Co and Ni,  $2\theta=65^\circ$  peak of Cr, Fe and Ni  $2\theta=76^\circ$  peak of Co and Ni,  $2\theta=78^\circ$  peak of Al and  $2\theta=84^\circ$  peak of Fe and Cr elements are present. These peaks' intensities are less than the intensity of the elemental peaks in the XRD test taken from the powder of these elements [25].

After 12 h of milling, peaks of alloying elements are observed with a noticeable decrease in intensity. With the increase of milling time, peaks broadening is apparent, and some peaks become invisible after 48 h. By increasing the mixing time to 36 h, the peaks are flattened. The vanishing of the peaks can indicate the formation of a solid solution phase. Although the elements' peaks are seen at first, with the increasing milling time, the peak intensity of the elements decreases. As a result, milling becomes effective. 36-hour milling produces only BCC peaks with peaks of some elements, such as Al and Ni. As the milling time increases to 48 h, only one peak is visible, confirming the formation of a complete solid solution phase. After milling for 48 h, the elemental peaks have vanished. An accumulated peak at  $2\theta = 44-45^\circ$  indicates the formation of a solid solution structure of

BCC. The formation of BCC phases in the alloy is due to powerful BCC forming elements such as Cr, Fe, Mn, and Al [42].

Three parameters use to evaluate the collective behavior of elements in a multi-component alloy system: the entropy of mixing ( $\Delta S_{mix}$ ), the enthalpy of mixing ( $\Delta H_{mix}$ ), and the atomic size difference parameter ( $\delta$ ). The values of  $\Delta S_{mix}$  and  $\Delta H_{mix}$  could be figured out based on the Boltzmann hypothesis and the Miedema model, respectively. Using these three parameters, the formation criteria for equiatomic high entropy solid solution can be summarized as the following:

- (1)  $\Delta S_{mix} \geq 1.61R$
- (2)  $\delta \leq 6.45$ :
- (3)  $-2.685\delta - 2.54 \leq \Delta H_{mix} \leq -1.28\delta + 5.44 \text{ kJ/mol}$ .

Adopted the three parameters and took another two into account: the electronegativity ( $\Delta\chi$ ) and the valence electron concentration (VEC), which were considered from the Hume-Rothery rules [18, 19]. Both  $\Delta\chi$  and VEC have weak effects on enhancing the formation of solid solution or amorphous phase. However, VEC plays a significant role in forming the FCC or BCC solid solution in high-entropy alloys, a large value of VEC ( $\geq 8$ ) promotes the formation of the FCC phase, while a smaller value leads to the BCC phase. The as-calculated values of  $\Delta S_{mix}$  ( $\text{JK}^{-1}\text{mol}^{-1}$ ),  $\Delta H_{mix}$  ( $\text{KJmol}^{-1}$ ), and  $\delta$  for AlCoCrFeMnNi high-entropy alloy are 1.61R, -11.89, and 5.56 respectively, which are highly consistent with the formation criteria.

Moreover, the extension of solid solubility is the main advantage of MA. Therefore, it is reasonable to infer that forming a simple solid solution for the MA-ed HEA is easier. According to the value of valence electron concentration, the solid solution type of AlCoCrFeMnNi high-entropy alloys is BCC, which has been confirmed by XRD analysis [42].

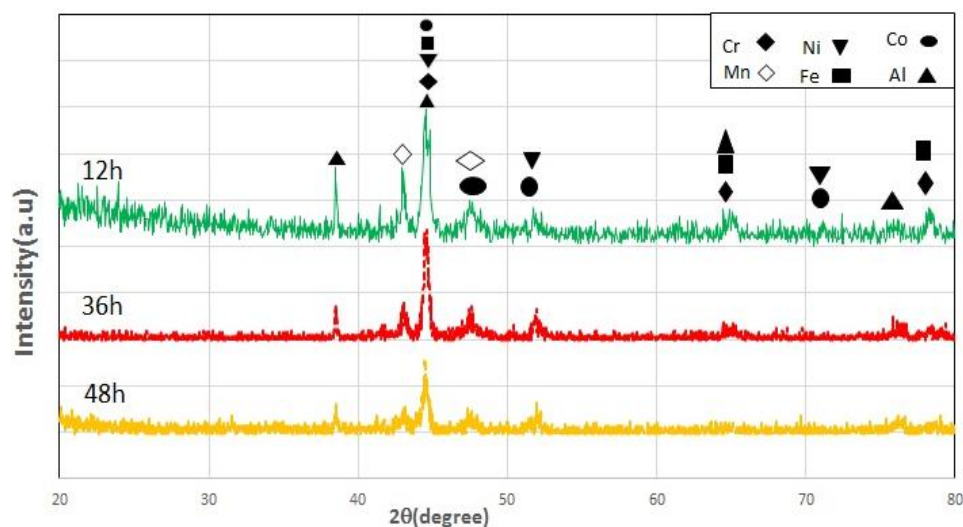


**Fig. 1.** XRD diagram of high entropy AlCoCrFeMnNi alloy powder with various milling times of 12 h, 36 h, and 48 h.

Along with the milling method, the decrement in intensity and the broadening of the peak may result from the three parameters: refined crystal size, high lattice strain, and decreased crystallinity. As a result of the mechanical alloying process, the diffraction peak vanishes due to 1) crystal refinement, 2) high lattice distortion, and 3) solid solution. The Scherer

formula measures the size of the crystals (CS) after different milling periods. Also, lattice strain (LS) was measured with the help of Expert High Score software. According to the Table 2, the size of the crystals and the strain of the lattice change with milling time.

**Table 2.** The crystal size (CS) and lattice strain (% LS) at different milling time.

Milling time (h)	CS (nm)	LS %
0	-	-
12	20	0.35
36	17	0.6
48	15	0.66

Table 2 illustrates the impression of milling time on the crystallinity of AlCoCrFeNiMn powders. Increasing the milling time resulted in a decrease in the crystal size. As the milling time increases, more particles will collide with each other and with steel balls. The rotation of the chamber at a speed of 120 RPM also causes an exponential increase in these collisions. 20 nanometers for 12 h of milling reaches 15 nm for 48 h of milling, which shows this decreasing trend. When collisions increase, energy is transferred to the atoms, which causes the placement of elements with different atomic radii in the crystal structure. So, the crystal stress and lattice strain increase.

The crystal strain increases from 0.35% in 12 h to 0.66% in 48 h of milling. It is actually due to the repeated collisions of the powder particles and balls. On the other hand, the network distortion increases to 0.66%. In the research of Ju *et al.* [42], the same results about lattice distortion have been reported. According to the Scherer formula, BCC peaks are low in intensity and the corresponding peaks widths' show a decrease in crystal size. It shows the alloying process is being completed after 48 h of milling. The nanoscale of crystallite size indicates that the micrometer-scale alloy particles have reached nanoscale-sized grains.

Figure 2 shows SEM images of powders. It can be seen the conversion in size, morphology, and agglomeration is a subordinate of milling time duration mechanical alloying. Al, Co, Cr, Fe, Ni, Mn element powders adhere to each other through cold welding by repeated collisions of steel balls. On average, the size of agglomerated powders increased after 12 h of milling. After 48 h, the particle size does not grow because of a balance between the cold welding and breaking of the welded powders. As shown in Figure 2 (a), micrometer-sized particles gradually adhere to each other through cold welding. As the milling time increases, more particles are welded to each other. This trend can be observed in Figure 2 (b,c). Figure (d,e) show the morphology of the particles after 48 h of milling, which is the final stage of mechanical alloying. It is shown that particles are fractured and have nanometer-scale sizes. This issue has also been obtained in the research of Wang *et al.* [42]. The size of the crystals and the strain of the lattice are measured after different milling times by the Scherer formula. They showed that after 30 h of mechanical alloying, the crystal size reaches 15 nm. Further increase in milling time has little effect on the crystal size, which indicates that equilibrium is achieved in mechanical alloying [42].

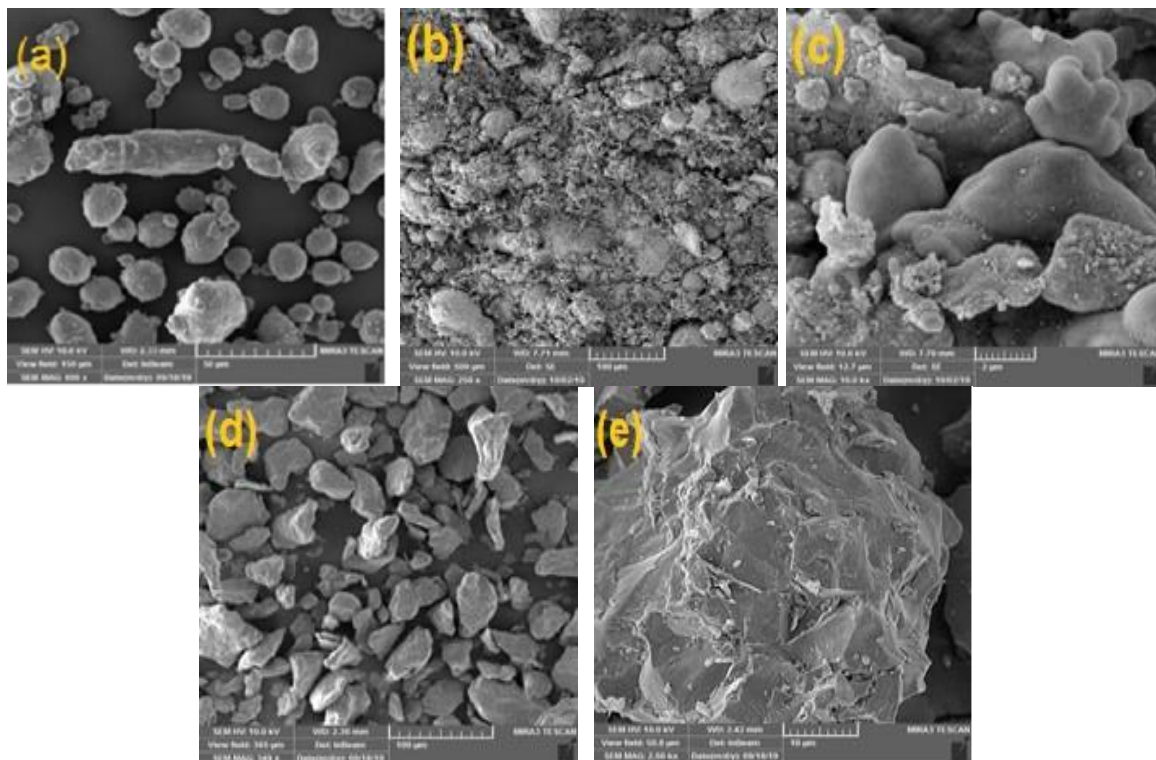


Fig. 2. SEM images of milled powders at different milling times (a) 12 h, (b,c) 36 h, and (d,e) 48 h.

### 3.2. Spark Plasma Sintered Specimens

To optimize the sintering temperature, experiments were done at 700, 900, and 1000 °C. Figure 3 shows the XRD pattern for spark plasma sintered specimens. In sintered sample at 700 °C, both BCC and FCC phases are detected. It is exciting that no intermetallic compounds were found in sintered high entropy alloy, which is desirable for mechanical properties in ambient temperature applications. The solid solution structure is composed of a structure consisting of BCC and FCC phases. The peak at  $2\theta=28^\circ$  is related to the element carbon, which results from the graphite used in the spark plasma sintering process.

The creation of a solid solution in a high entropy alloy relates to the entropy of mixing ( $\Delta S_{mix}$ ), enthalpy of mixing ( $\Delta H_{mix}$ ), atomic size difference parameter ( $\delta$ ), electronegativity ( $\Delta\chi$ ) and electronic valance configuration (VEC). The theoretical calculation of these parameters was made on AlCoCrFeNiMn high entropy alloy. The value of  $\Delta S_{mix}$ ,  $\Delta H_{mix}$ ,  $\delta$ ,  $\Delta\chi$ , and VEC was apperceived to be  $1.79R JK^{-1} mol^{-1}$ ,  $-11.67 KJ mol^{-1}$ , 5.56, 1.2843, 7.1638, respectively. According to the listed parameters, the phase formation of AlCoCrFeNiMn high entropy alloy could be a mixture of both FCC and BCC solid solution, which complies with the XRD pattern outcome after sintering (Figure 3) [43].

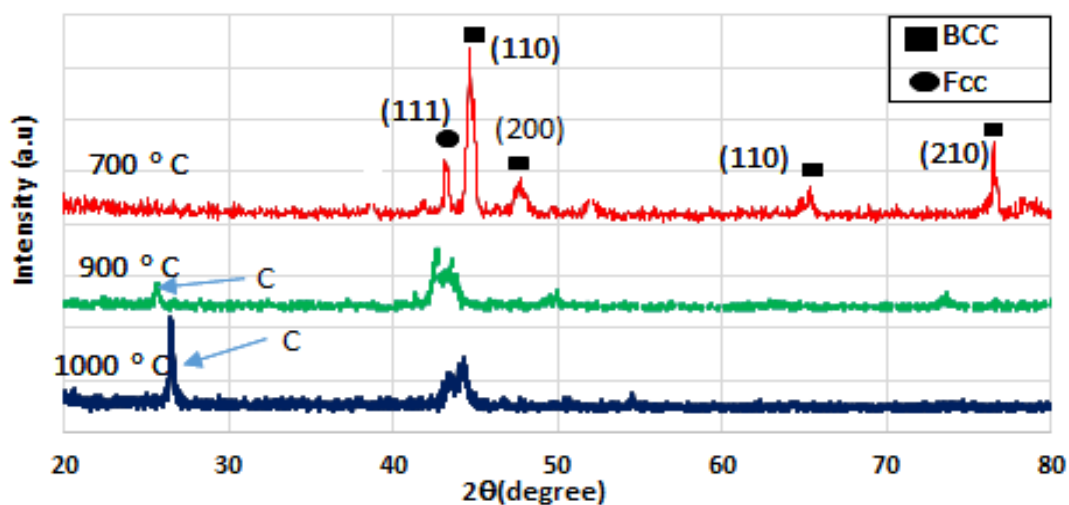
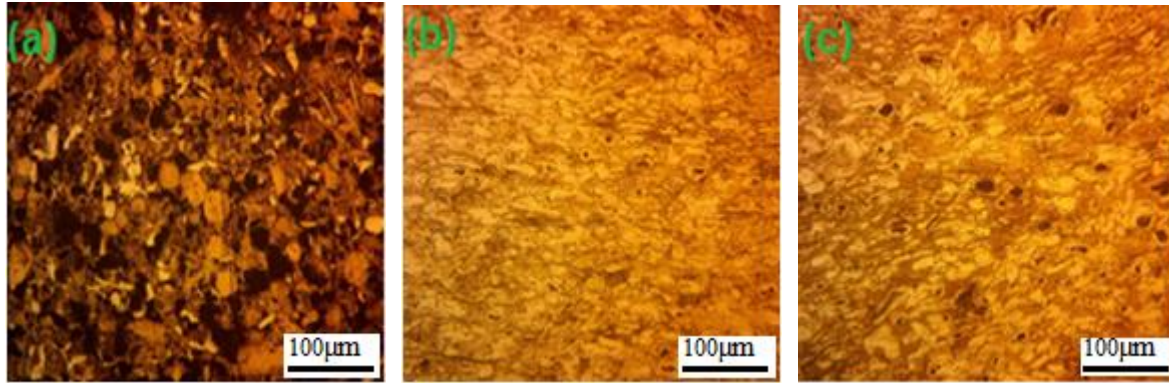


Fig. 3. XRD pattern of high entropy AlCoCrFeMnNi alloy powder at different sintering temperatures of 700, 900, and 1000 °C.

Figure 4 shows the microstructure of AlCoCrFeNiMn alloy sintered via the SPS process. These images show the metallographic images of spark plasma sintered alloy after it had been ball milled for 48 h. The formation of two phases with white and gray colors is clearly seen. Also, it is obviously seen very fine; dark color particles are dispersed in between dendrite. It seems that the structure in Figure 4 (c) is larger compared to Figure

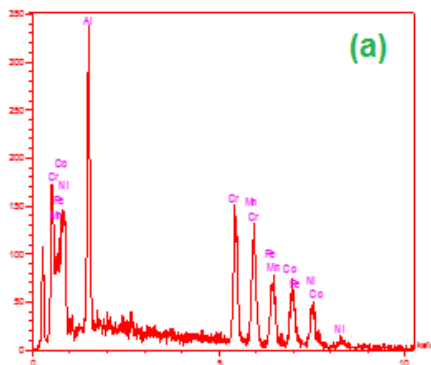
4 (a,b). The reason is the occurrence of secondary grain growth at 1000 °C. The dark dispersed particles are graphite particles that are introduced during the SPS process and form some compounds with chromium. This is a chromium carbide compound that the graphite used in the sintering process penetrates due to the high penetration speed and combines with the chromium alloy element.



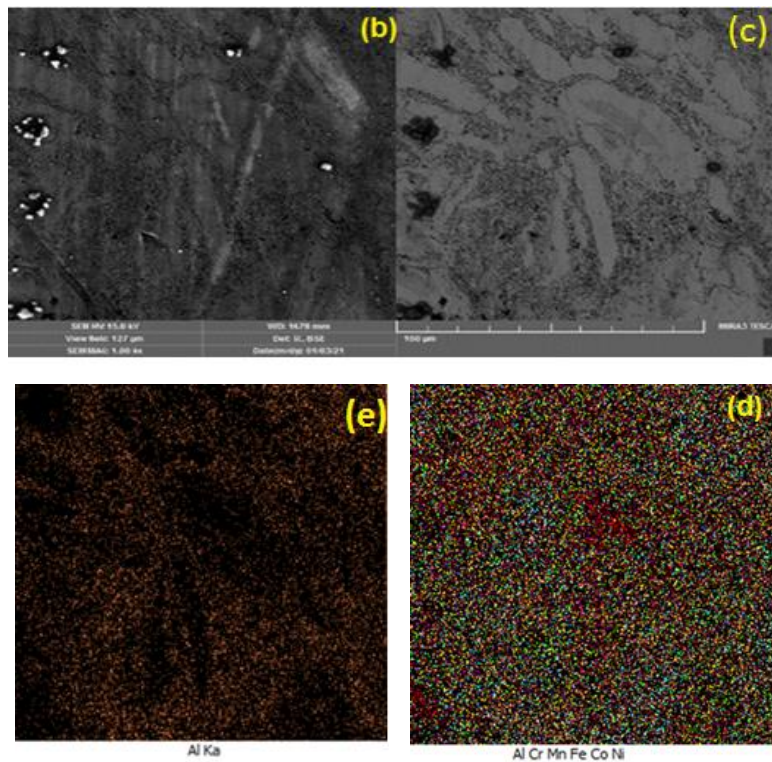
**Fig. 4.** Metallographic of AlCoCrFeMnNi alloy after sintering at different temperatures of (a) 700, (b) 900 and (c) 1000 °C.

Figure 5 shows the secondary electron image (SE), EDS, and map analysis of powders milled for 48 h and sintered by SPS. The images show that there are three areas with light and dark gray and black colors. Based on the EDS analysis of dark gray areas, the intensity of aluminum is higher there. The distribution of elements can be seen in the map analysis. It shows that these areas have more aluminum. The weight percentage of aluminum is 20.53 percent in this area. The region with 7.7wt % Cr is actually the BCC phase, which has the element of aluminum as the main phase. Aluminum's large atomic size prevents it from fitting into the structure of the FCC, which causes the formation of the BCC phase. The grain size is calculated at different

sintering temperatures. At a sintering temperature of 700 °C, the grain size of the white phase is 30.7 μm and the grain size of the gray phase is 28.8 μm. At 900 °C, the grain sizes become 19.2 μm and 18.8 μm, respectively. At 1000 °C sintering temperature, the white phase grain size is 23 micrometers and the gray phase grain size is 21.3 micrometers. It is observed that with increasing the temperature, at first, a decrease in grain size is observed, and then at 1000 °C, a little increase in grain size could be seen. This decrease could be due to the bonding of different particles in the sintering process and the formation of new grain boundaries. The subsequent increase in grain size can be due to the increase in temperature and grain growth.



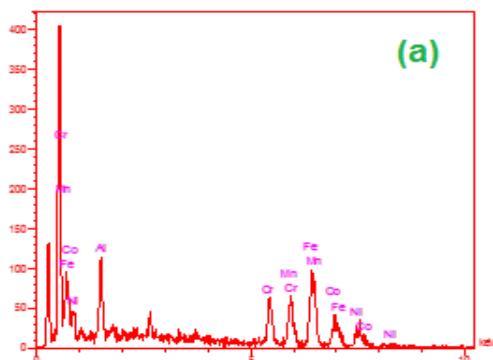
Elt	Line	Int	Error	K	Kr	W%	A%
Al	Ka	625.10	0.82	0.13	0.12	20.53	35.25
Cr	Ka	117.60	0.71	0.09	0.08	7.70	6.87
Mn	Ka	241.90	0.71	0.22	0.20	19.08	16.09
Fe	Ka	72.20	0.71	0.08	0.07	6.98	5.79
Co	Ka	168.40	0.71	0.23	0.20	21.79	17.13
Ni	Ka	150.60	0.71	0.26	0.23	23.93	18.88
				1.00	0.90	100.00	100.00



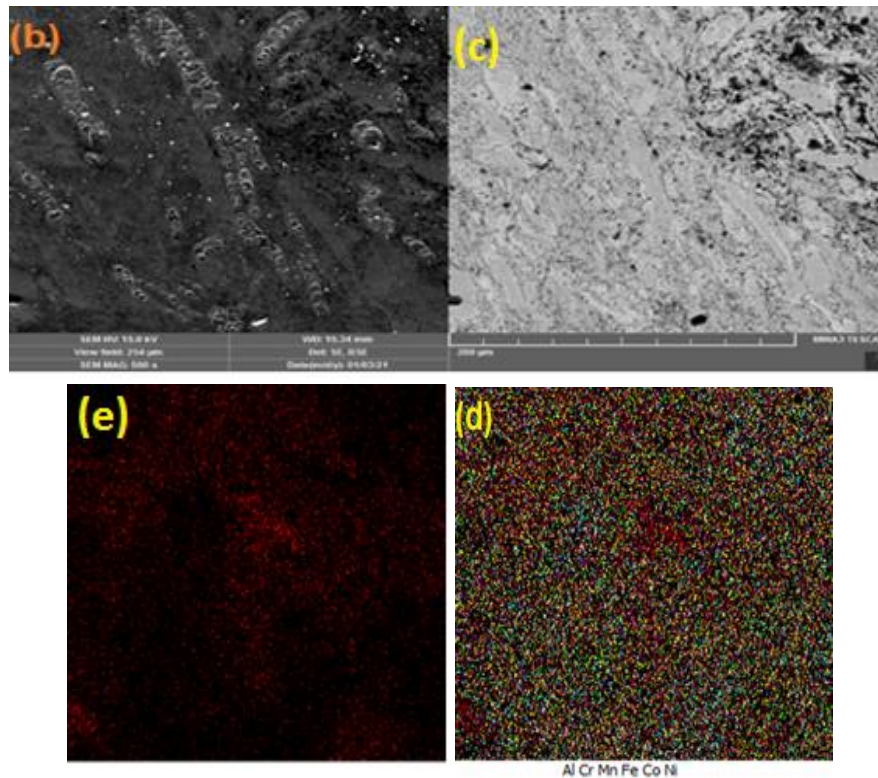
**Fig. 5.** (a) EDS of the dark gray zone at AlCoCrFeMnNi alloy powder sintered at 900°C. (b) and (c) Microstructure secondary image (SE) and, (e)-(d) map image of the dark gray zone at AlCoCrFeMnNi alloy powder sintered at 900°C.

Figure 6 shows the secondary electron image (SE), EDS, and map analysis of powders milled in 48 h and sintered by SPS. The images show that there are some areas with a light gray zone. According to the EDS analysis performed on light gray areas, the intensity of Cr is higher in this area. From the map analysis, the distribution of elements can be seen very easily. It illustrated that these areas have more Cr. The weight percentage of Cr is 19.29%. The region with 9.02 wt.% Al is actually the FCC phase, which has the element of Cr as the main phase. According to XRD patterns, AlCoCrFeNiMn alloy contains FCC

and BCC phases. Some areas of microstructure have a dark area due to the fine size and the existence of the third carbide phase. The white phase is the exactly rich zone from Cr and has the HEA alloy composition. The dark gray phase has an Al and Ni-rich concentration which can be identified as the B2 phase, and the dark spots are the areas rich in Cr, which can be chromium carbide ( $Cr_3C_{27}$ ). The carbon introduction occurs from the graphite crucible used in the sintering process. Carbon diffusion usually occurs rapidly. Carbide phases are often found in alloys obtained from the SPS process.



Elt	Line	Int	Error	K	Kr	W%	A%
Al	K a	276.00	0.99	0.05	0.05	9.02	17.03
Cr	K a	311.10	1.03	0.21	0.20	19.29	18.91
Mn	K a	229.90	1.03	0.19	0.18	17.60	16.32
Fe	K a	201.20	1.03	0.20	0.19	19.11	17.44
Co	K a	142.40	1.03	0.17	0.17	17.70	15.30
Ni	K a	112.60	1.03	0.17	0.17	17.28	15.00
				1.00	0.96	100.00	100.00



**Fig. 6.** (a) EDS, (b), (c) Microstructure secondary image (SE) and, (e) and (d) map image of the light gray zone at AlCoCrFeMnNi alloy powder sintered at 900°C.

The relative density and hardness of the alloy were measured after sintering at these temperatures. Figure 7 shows the relative density of spark plasma sintered specimens. The measured relative densities of all samples are larger than 99%, indicating they have reached near theoretical density. It is seen that the relative density enhances significantly from 700 to 900 °C. But a slight increase is seen from 900 to 1000

°C. At 1000°C, rapid grain growth stops, leading to a low increase in density. The increase in temperature caused by grain growth, elimination of grain boundaries, and loss of space between boundaries results in decreased porosity between grains and increased density. Although the highest density is attained at 1000 °C, the slope of density is decreased.

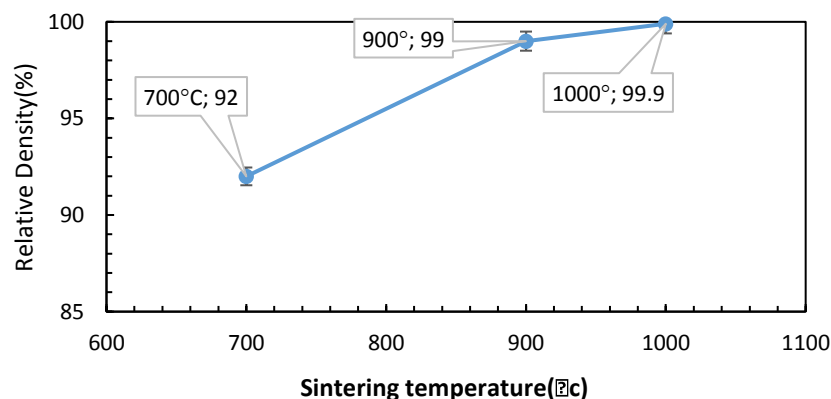


**Fig. 7.** Relative density of AlCoCrFeNiMn alloy at different sintering temperatures.

Figure 8 shows the hardness of sintered specimens. The hardness increased from 700 to 900 °C and then gradually decreased from 900 to 1000 °C due to the phenomenon of grain growth when HEAs are produced by powder metallurgy, grain refinement is accomplished during the mechanical alloying process. In the sintering step, these particles are kept

smaller. Increasing the lattice distortion in mechanical alloying increases mechanical properties. Solid solution and the emergence of a BCC solid-phase increase the hardness to 649 Vickers. The hardness of 527 Vickers is achieved at 1000 °C due to slight grain growth with a slight decrease in hardness.

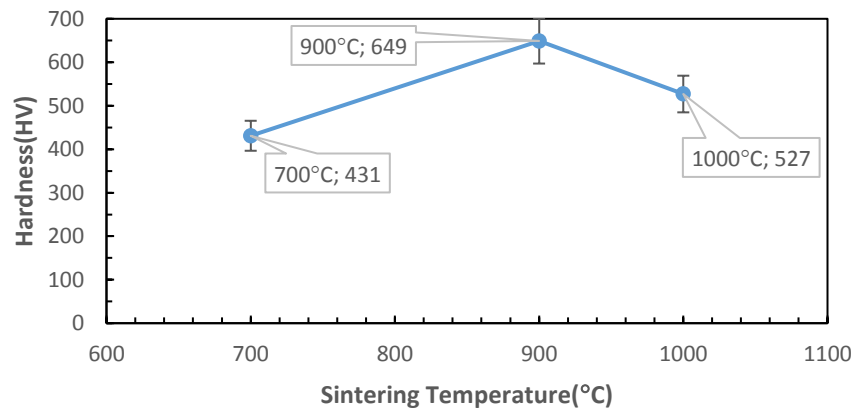


**Fig. 8.** Hardness of AlCoCrFeNiMn sintered alloy at different sintering temperatures.

It can be stated that the high entropy alloy of AlCrCoFeMnNi, which has a hardness of about 650 HV, will have good abrasion resistance. According to the Archard equation, the wear rate value is inversely related to the amount of hardness. The expectation is that alloys with higher hardness will have lower wear rates [44].

Cr is an important compound in HEA alloys and in the case of alloys with the equiatomic elements, Cr stabilizes the BCC structure and plays an important role in the mechanical properties of the alloy. The presence of Cr, Fe, Co elements that have the BCC structure at room temperature usually promotes the formation of the BCC phase. With the formation of the BCC phase, it is often seen an improvement in mechanical properties. The hardness of AlCoCrFeMnNi high entropy alloy also depends on the microstructure of the alloy. When the structure changes from a two-phase to a one-phase solid solution structure, the hardness increases, and this change improves the wear resistance [45].

#### 4. Conclusions

In this study, AlCoCrFeNiMn alloy was prepared by milling and then SPS sintering process. Process parameters such as milling time and sintering temperature were optimized to get good results in an alloy with a high entropy single phase. 1) Milling times were selected as 12 h, 36 h, and 48 h, respectively. Based on the results, after 48 h of milling a high entropy alloy with a single solid solution structure was produced by mechanical alloying. The same phase is achieved in 48 h of milling. The optimum time to reach the alloy with the desired structure and properties was determined as 48 h. Also, the sintering operation was performed by spark plasma sintering at temperatures of 700, 900, and 1000 °C. 2) According to the XRD patterns and SEM images of the obtained structure, it consists of two-phase, chromium-rich FCC, and aluminum-rich

BCC phase. Also, black carbide compounds are formed due to the introduction of graphite used in the SPS process and its combination with carbide-forming elements such as chromium. 3) If the density is a factor, then 1000 °C is the optimum sintering temperature since the density is 99.9% of the theoretical density. 4) The highest hardness is achieved at 900 °C sintering and is equal to 649 HV<sub>0.05</sub>.

#### Declarations

There's no financial/personal interest or belief that could affect the objectivity, data, and nature of the manuscript. Also, this manuscript has no associated data. All data are given in the text.

#### Reference

- [1] S. K. Tang, *The Process Fundamentals and Parameters of Electro-Spark Deposition*, Waterloo, Ontario, Canada, 2009.
- [2] Environmental Security Technology Certification Program (ESTCP), *Electrospark Deposition for Depot- and Field-Level Component Repair and Replacement of Hard Chromium Plating*, U.S. Department of defense, Project WP-0202, 2006.
- [3] E. sharghivand, H. Aghajani, M. Roostaei: *FeNiCrAlCoMn High Entropy Alloy Coating Prepared on Ti6Al4V by ESD*, Imat 2018, Tehran, Iran, 2018.
- [4] D. Liu, W. Gao, Z. Li, H. Zhang and Z. Hu, *Electro-spark deposition of Fe-based amorphous alloy coatings*, *Materials Letters* 61 (2007) 165–167.
- [5] S. Praveen, H.S. Kim, *High- Entropy Alloys: Potential candidates for High-Temperature Applications-An Overview*, *Adv. Eng.Mater.* 20 (2018) 1700645.
- [6] W. Li, P. L., Peter K. Liaw, *Microstructure and properties of high-entropy alloy films and coatings: a review*, *Mater. Res. Lett*, 6 (2018) 199-229.

- [7] N. Stepanoy, M. Tikhonovsky, N. Yurchenko, D. Zyubkin, M. Klimova, S. Zherebstove, A. Efenov, G. Salishchev, "Effect of cryo-deformation on structure and properties of CoCrFeMnNi high-entropy alloy, *Intermetallics*, 2015, 59, 8-17.
- [8] B. Sckuh, F. Mendez-Martin, B. Volker, E.P. George, H. Clements, R. Pipan, A. Hohenwarter, Mechanical properties, microstructure and thermal stability of a nanocrystalline CoCrFeMnNi high-entropy alloy after sever plastic deformation, *Acta Mater.* 96 (2015) 258-268.
- [9] M-R. Chen, S-J. Lin, J-W. Yeh, M-H. Chung, S-K. Chen, Y-S. Huang, Effect of vanadium addition on the microstructure, hardness, and wear resistance of Al<sub>0.5</sub>CoCrFeMnNi high-entropy alloy, *Metal. Mater. Trans. A* 37 (5) (2006), 1363-1369.
- [10] J. Y. He, W. H. Liu, H. Wang, Y. Wu, X.J. Liu, T. G. Nieh, Z.P. Lu, Effects of Al addition on structural evolution and tensile properties of the CoCrFeMnNi high-entropy alloy system, *Acta Mater.* 62 (2014) 105-113.
- [11] T. Borkar, B. Gwalani, D. Chudhuri, C. V. Mikler, C.J. Yannerta, Xianodong Chen, ghavan Ramanujan, M. J. Styles, M. A. Gibson, R. Banerjee, A combinatorial assessment of Al<sub>X</sub>CrCuFeNi<sub>2</sub> (0 < X < 1.5) complex concentrated alloys: microstructure, microhardness, and magnetic properties, *Acta Mater.* 116 (2016) 63-76.
- [12] B. Gwalani, V. Soni, D. Choudhuri, M. Lee, J. Y. Hwang, S. J. Nam, H. Ryu, S. H. Hong, R. Banerjee, Stability of ordered L12 and B2 precipitates in face centered cubic based high entropy alloys-Al<sub>0.3</sub>CoFeCrNi and Al<sub>0.3</sub>CuFeCrNi<sub>2.5</sub>Cr. *Mater.* 123 (2016) 130-134.
- [13] W. H. Liu, Y. Wu, J. Y. He, T. G. Nieh, Z. P. Lu, Grain growth and Hall-Petch relationship in a high-entropy FeCrMnNiCoMn alloy, *Scr. Mater.* 68 (7) (2013) 526-529.
- [14] J. W. Yeh, S. K. Chen, S. J. Lin, J. Y. Gan, T. S. Chin, T. T. Shun, C. H. Tsau, S. Y. Chang, Nanostructured high-entropy alloys with multiple principal elements: Novel alloy design concepts and outcome, *Adv. Eng. Mater.* 6 (2004) 299-303.
- [15] B. Cantor, I.T.H. Chang, P. Knight, A. J. B. Vincent, Microstructural development in equiatomic multicomponent alloys, *Mater. Sci. Eng. A*. 375-377 (2004) 213-218.
- [16] C. J. Tong, M. R. Chen, S. K. Chen, J. W. Yeh, T. T. Shun, S.J. Lin, S. Y. Chang, Mechanical perform of The Al<sub>X</sub>CrCoCuFeNi High-Entropy Alloy System with Multiprincipal Elements, *Metall. Mater. Tran. A*. 36 (2005) 1263-1271.
- [17] P. K. Huang, J. W. Yeh, T. T. Shun, S. K. Chen, Multi-Principal Element Alloy
- [18] With Improved Oxidation and Wear resistance for thermal Spray Coating, *Adv. Eng. Mater.* 6 (2004) 74-78.
- [19] C. Y. Hsu, J. W. Yeh, S. K. Chen, T.T. Shun, Wear resistance and high-temperature compression strength of FCC CuCoNiCrAl<sub>0.5</sub> alloy with boron addition, *Metal. Mater. Trans. A*. 35 (2004) 1465-1469.
- [20] K. B. Zhang, Z. Y. Fu, J. Y. Zhang, W. M. Wang, S. W. Lee, K. Niihara, Characterization of nanocrystalline CoCrFeNiTiAl high-entropy solid solution processed by mechanical alloying, *J. Alloys Compd.* 495(2010) 33-38.
- [21] S. Singh, N. Wanderka, B. S. Murty, U. Glatzel, J. Banhart, Decomposition in multi-component AlCoCrCuFeNi high-entropy alloy, *Acta Mater.* 59 (2011) 182-190.
- [22] S. Praveen, A. Anupam, T. Sirasani, B. S. Murty, R. S. Kottada, Characterization of oxide dispersed AlCoCrFe high entropy alloy synthesized by mechanical alloying spark plasma sintering, *Trans. Indian Inst. Met.* 66 (2013) 369-373.
- [23] Y. Zhang, T. T. Zuo, Z. Tange, M. C. Gao, K. A. Dahmen, P. K. Liaw, Z. P. Lu, Microstructure and properties of high-entropy alloys, *Prog. Mater. Sci.* 61 (2014) 1-93.
- [24] F. Otto, A. Dlouhy, C. Somsen, H. Bei, G. Eggeler, E. P. George, The influences of temperature and microstructure, on the tensile properties CoCrFeMnNi high-entropy alloy, *Acta Mater.* 61(15) (2013) 5743-5755.
- [25] M. Roostaei, H. Aghajani, M. Abbasi and B. Abasht, Formation of Al<sub>2</sub>O<sub>3</sub>/MoS<sub>2</sub> nanocomposite coatings by the use of electro spark deposition and oxidation, *Ceramics International*, 47 (2021) 11644-53.
- [26] X. R. Tan, G. P. Zhang, Q. Zhi, and Z.X. Liu, Effects of milling on the microstructure and hardness of Al<sub>2</sub>NbTi<sub>3</sub>Zr high-entropy alloy. *Mater. Des.* 109 (2016) 27-36.
- [27] M. Vaidya, A. Marshal, K. G. Ppradeep, and B. S. Murty: Phase evolution and stability of nanocrystalline CoCrFeNi and CoCrFeMnNi high entropy alloys. *J. Alloys Compd.* 770, (2019) 1004-15.
- [28] W. Ji, W. Wang, H. Wang, J. Zhang, Y. Wang, F. Zhang, and Z. Fu, Alloying behavior and novel properties of CoCrFeMnNi high-entropy alloy fabricated by mechanical alloying and spark plasma sintering. *Intermetallics* 56 (2014) 24-7.
- [29] J. Y. He, W. H. Liu, H. Wang, Y. Wu, X. J. Lui, T. G. Nieh, Z. P. Lu, Effects of Al addition on structural evolution and tensile properties of the FeCoNiCrMn high-entropy alloy system, *Acta Mater.* 62 (2014) 105-113.

- [30] C. Wang, W. Ji, Z. Fu, Mechanical alloying and spark plasma sintering of CoCrFeNiMnAl high-entropy alloy, *Adv. Powder Technol.* 25 (2014) 1334-1338.
- [31] W. Ge, B. Wu, S. Wang, S. Xu, C. Shang, Z. Zhang, and Y. Wang, Characterization and properties of CuZrAlTiNi high entropy alloy coating obtained by mechanical alloying and vacuum hot pressing sintering. *Adv. Powder Technol.* 28 (2017) 2556-63.
- [32] Y. Xie, H. Chang, Q. Tang, W. Chen, W. Chen, and P. Dai, Effects of N addition on microstructure and mechanical properties of CoCrFeNiMn high entropy alloy produced by mechanical alloying and vacuum hot pressing sintering. *Intermetallics* 93 (2018) 228-34.
- [33] H. Cheng, W. Chen, X. Liu, Q. Tang, Y. Xie, and P. Dai, Effect of Ti and C additions on the microstructure and mechanical properties of the FeCoCrNiMn high-entropy alloy. *Mater. Sci. Eng., A* 719 (2018) 192-8.
- [34] S. Varalakshmi, M. Kamaraj, and B. S. Murty, Processing and properties of nanocrystalline CuNiCoZnAlTi high entropy alloys by mechanical alloying. *Mater. Sci. Eng. A* 527 (2010) 1027-30.
- [35] Z. Fu, W. Chen, Z. Chen, H. Wen, and E. J. Lavernia, Influence of Ti addition and sintering method on microstructure and mechanical behavior of a medium-entropy Al<sub>0.6</sub>CoNiFe alloy. *Mater. Sci. Eng. A* 619 (2014) 137-45.
- [36] V. Shivam, J. Basu, Y. Shadangi, M. K. Singh, and N. K. K. Mukhopadhyay: Mechano-chemical synthesis, stability and phase evolution in AlCoCrFeNiMn high entropy alloy. *J. Alloys Compd.* 757 (2018) 87-97.
- [37] S. Varalakshmi, G. Appa Rao, M. Kamaraj, and B. S. Murty: Hot consolidation and mechanical properties of Nano crystalline equiatomic AlFeTiCrZnCu high entropy alloy after mechanical alloying. *J. Mater. Sci.* 45 (2010) 5158-63.
- [38] S. Praveen, B. S. Murty, and R. S. Kottada: Alloying behavior in multi-component AlCoCrCuFe and NiCoCrCuFe high entropy alloys. *Mater. Sci. Eng., A* 534 (2012) 83-9.
- [39] M. Vaidya, M. Murakhnshina Garlopal: High-entropy alloys by mechanical alloying: A review, *Mater. Res.* 34 (2019) 664-86.
- [40] S. Praveen, A. Anupam, T. Sirasani, B. S. Murty, and R. S. Kottada: Characterization of oxide dispersed AlCoCrFe high entropy alloy synthesized by mechanical alloying and spark plasma sintering. *Trans. Indian Inst. Met.* 66 (2013) 369-73.
- [41] E. Colombini, R. Rosa, L. Trombi, M. Zadra, A. Casagrande, and P. Veronosi, High entropy alloys obtained by field assisted powder metallurgy route: SPS and microwave heating. *Mater. Chem. Phys.* 210 (2018) 78-86.
- [42] C. Wang, Wei Ji, Zhengyi Fu: Mechanical alloying and spark plasma sintering of CoCrFeMnNiAl high-entropy alloy, *Advanced Powder Technology.* 25 (2014) 1334-8.
- [43] H. Prasad, Sh. Singh, B. B. Panigrahi: Mechanical activated synthesis of Alumina dispersed FeNiCoCrAlMn high entropy alloy. *J. Alloys Compd.* 692 (2017) 720-6.
- [44] J. W. Yeh, S. J. Lin, Breakthrough applications of high-entropy materials. *J. Mater. Res.* 33 (2018) 3129-37.
- [45] L. QH, Y. TM, G. ZN, et al. Microstructure and corrosion properties of AlCoCrFeNi high entropy alloy coatings deposited on AISI 1045 steel by the electrospark process. *Metal Mater Trans A.* 44 (2012) 1767-1778.